In vivo evaluation of optic nerve aging in adult rhesus monkey by diffusion tensor imaging

Yumei Yan[1], Longchuan Li[2], Todd M. Preuss[3], Xiaoping Hu[4], James G. Herndon[3], Xiaodong Zhang[1,3]

[1]Yerkes Imaging Center, Yerkes National Primate Research Center, Emory University, Atlanta, Georgia 30329, USA; [2]Marcus Autism Center, Children's Healthcare of Atlanta, Emory University, Atlanta, Georgia 30322, USA; [3]Division of Neuropharmacology and Neurologic Diseases, Yerkes National Primate Research Center, Emory University, Atlanta, Georgia 30329, USA; [4]The Wallace H. Coulter Department of Biomedical Engineering, Emory University and Georgia Institute of Technology, Atlanta, Georgia 30322, USA

Corresponding to: Xiaodong Zhang, Ph.D. 954 Gatewood Rd NE, Atlanta, GA 30329, USA. Email: xzhang8@emory.edu.

Abstract: Aging of the optic nerve can result in reduced visual sensitivity or vision loss. Normal optic nerve aging has been investigated previously in tissue specimens but poorly explored *in vivo*. In the present study, the normal aging of optic nerve was evaluated by diffusion tensor imaging (DTI) in non-human primates. Adult female rhesus monkeys at the ages of 9 to 13 years old (young group, n=8) and 21 to 27 years old (old group, n=7) were studied using parallel-imaging-based DTI on a clinical 3T scanner. Compared to young adults, the old monkeys showed 26% lower fractional anisotropy (P<0.01), and 44% greater radial diffusivity, although the latter difference was of marginal statistical significance (P=0.058). These MRI findings are largely consistent with published results of light and electron microscopic studies of optic nerve aging in macaque monkeys, which indicate a loss of fibers and degenerative changes in myelin sheaths.

Keywords: Optic nerve aging; white matter; mean diffusivity (MD); fractional anisotropy (FA); non-human primate; parallel imaging; GRAPPA

Introduction

The optic nerve is the continuation of the axons of ganglion cells in the retina, and the pathway by which visual information is transferred from the retina to the visual cortex. Aging of the optic nerve can result in reduced visual sensitivity or vision loss due to reduction of retinal ganlion cells and nerve fibers (1-3). As seen in glaucoma, progressive neurodegeneration of retinal ganlion cells and axons can lead to irreversible loss of visual sensitivity or blindness (4-7). Normal optic nerve aging has been studied previously using light and electron microscopic methods on specimens from humans (1,8), monkeys (9-11) and rats (12). *In vivo* investigation of the optic nerve, beyond the intraocular optic nerve head, has been hindered in the past because the nerve could not be assessed non-invasively. In recent years, high-field MRI and fast imaging techniques have facilitated both animal research and clinical investigation dramatically, and MRI has been increasingly used in various studies of

visual pathways, thus helping to overcome these difficulties.

Diffusion tensor imaging (DTI) (13) is a non-invasive MRI technique for characterizing white matter fiber tracts and has been used widely to investigate white matter development, integrity and aging in human brains (14-23). In recent years, it has been applied in *in vivo* studies of the optic nerve of humans (24-34), monkeys (35,36), rodents (25,37-40), demonstrating that DTI can be a robust means to non-invasively examine optic nerve organization and abnormalities.

Although rodent models of eye-related diseases are widely used (12,25,37,39-42), their visual system is markedly different from that of humans. In contrast, the visual system organization of nonhuman primates (NHPs), while not identical to that of humans, is much more human-like than that of rodents (43). Therefore, NHP models are particularly valuable for investigating the aging and neuropathology of the visual pathway (9,10,42,44,45). The aim of the present

www.amepc.org/qims

study was to evaluate the diffusion property changes during the normal optic nerve aging in adult rhesus macaque monkeys by DTI in a clinical 3T setting.

Materials and methods

Animal preparations

Fifteen young adult (9 to 13 years old, n=8) and old adult (21 to 27 years old, n=7) female rhesus monkeys were used in this study. Females were selected in order to minimize possible bias from gender difference because the nerve fiber degeneration with age may be different in male and female (46). Also, comparable sets of male macaques were not available to us for scanning at the time of the study.

The animals were initially anesthetized with ketamine (5-10 mg/kg, IM), then orally intubated and anesthetized with 1-1.5% isoflurane mixed with 100% O_2 during scanning. An IV catheter was placed for delivering lactated ringers solution (3.5-10 mL/kg/hr). The body temperature was maintained at 37.5 ℃ by a feedback-regulated circulating warm-water blanket. The anesthetized animals breathed spontaneously, and were immobilized with a custom-made head holder and placed in the "supine" position in the scanner. Et-CO_2, inhaled CO_2, O_2 saturation, blood pressure, the mean arterial pressure (MAP), heart rate, respiration rate, and body temperature were monitored continuously and maintained in normal range (47), in addition to visual inspection of animals at least every 30 minutes. All procedures were approved by the Institutional Animal Care and Use Committee (IACUC) of Emory University in accordance with the NIH Guide for Care and Use of Laboratory Animals.

MRI examination

MRI scans were performed on a Siemens TIM™ Trio 3T whole body scanner (Siemens Medical Solutions, PA, USA) with an 8-channel phase-array volume coil (INVIVO, Orlando, FL, USA). A double spin-echo single-shot echo-planar imaging (EPI) sequence with GRAPPA (Acceleration factor R =3) was utilized with the acquisition parameters: TR =7,000 ms/TE =108 ms, FOV =141 mm × 132.26 mm (93.8% phase FOV), data matrix =128×120, 1.1 mm isotropic resolution, b-value =0, 1,000 s/mm², 60 gradient directions, and ten averages [5-pairs of phase reversal acquisition (48)] including five b0 scans in each repetition. The phase reversal acquisition was conducted by

flipping the phase encoding direction by 180 degree in every other DTI scan. The total DTI acquisition time was about 86 minutes. High-resolution (0.5 mm isotropic resolution) T1-weighted images were acquired for structural identification of the optic nerve and for measuring optic nerve diameters. The T1-weighted images were collected using an MPRAGE sequence with GRAPPA (R =2) and the acquisition parameters: TR =2,600 ms, TE =3.37 ms, TI =900 ms, FOV =160 mm × 160 mm, data matrix =320×320, flip angle =8 degree, 0.5 mm slice thickness, 176 slices, and 3 averages.

Data analysis

DTI data from each animal were distortion-corrected, motion-corrected and averaged for generating MD (*Figure 1A*), FA (*Figure 1B*), axial diffusivity (AD or $\lambda_\parallel$) and radial diffusivity (RD or $\lambda_\perp$) maps using FSL 4.1.3 (http://www.fmrib.ox.ac.uk/fsl/). All the maps were interpolated in the three dimensions by a factor of 2 to facilitate subsequent data analysis. Using MRIcro 1.4 (http://www.mricro.com), regions of interest (ROIs) were selected manually on the coronal MD maps (*Figure 1A*, *bottom image*). The ROI or pixels of interest on each optic nerve consisted of a set of consecutive pixels located in the central section of the optic nerve, between its anterior and posterior quarters (*Figure 1C*). Also, the ROIs in each animal were cross-verified visually in three-dimensional views of their corresponding FA maps and b0 images (*Figure 1B* and *1D*). As no significant difference was observed between the left and right optic nerves (see Results for more details), the values of MD, FA, AD and RD in the corresponding ROIs of the two sides were averaged before statistical analysis. The interpolation and mean value calculation were implemented with Matlab (The MathWorks, Inc., MA, USA) scripts developed in-house. Probabilistic tractography analysis was performed using FSL with two masks defined on the coronal plane of FA map: one mask was set in the optic nerve at the midpoint between the eyeball and the optic chiasm, and the other one was 2.2 mm anterior to that point, toward the eyeball (*Figure 1D*). Also, the trackability of each optic nerve was examined by sending virtual streamlines from one of the two seed masks and counting the streamlines that reached to the other one and repeating the procedure with the seed mask order switched. The cross-sectional diameters at the middle section of the optic nerves were measured on T1-weighted images (*Figure 1E*) with ImageJ (http://imagej.nih.gov/ij). DTI measures for the left and right optic nerves were compared by means of the Student's paired *t*-test to determine whether
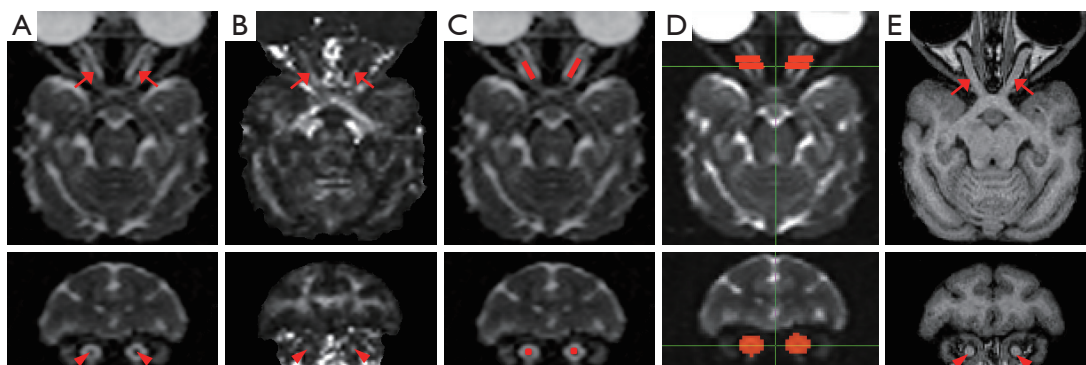
Figure 1 Illustration of optic nerve and regions of interest in the axial and coronal MRI images of an adult rhesus monkey. (A) Mean diffusivity (MD); (B) fractional anisotropy (FA) maps (both in 0.65 mm isotropic resolution after interpolation) of the same animal; (C) Region of interest (ROI) overlaid on the MD map. The ROI was selected manually between the anterior and posterior quarters of the optic nerve (see the axial image at the top), only including the central pixels of the optic nerve cross-sections (see the coronal image at the bottom) on the selected slices; (D) The two masks for optic nerve fiber tractography were selected on the middle slice (coronal image) of the optic nerves between the optic chiasm and retina, and 2.2 mm away from the middle slice, toward the eyeball; (E) T1 weighted images (0.5 mm isotropic resolution) of the optic nerve. The optic nerves are marked with arrows on the axial image at the top and on the coronal image at the bottom.
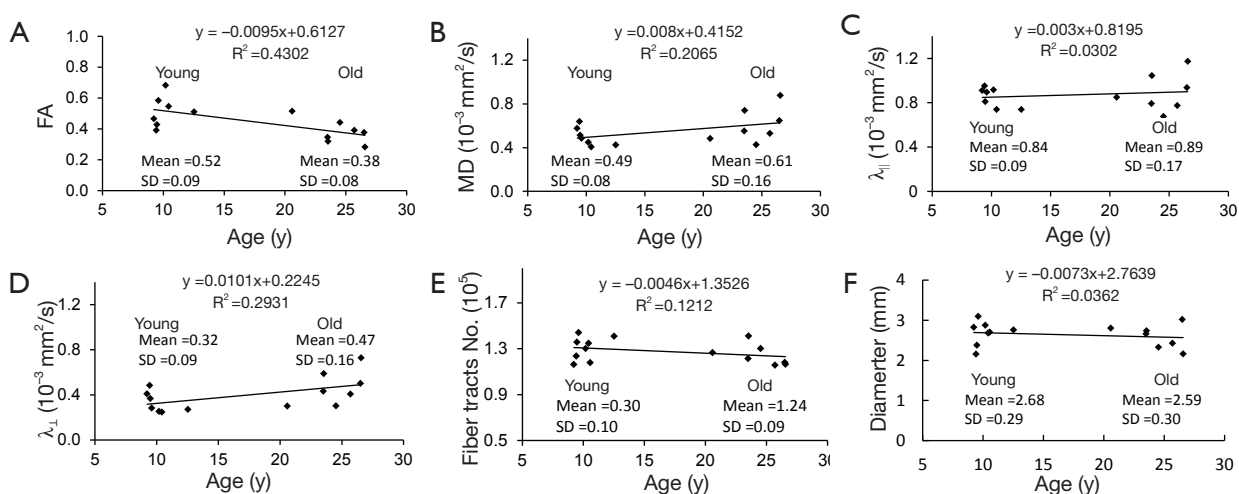

Figure 2 Age-related quantitative MRI changes in (A) fractional anisotropy (FA); (B) mean diffusivity (MD); (C) axial diffusivity (AD or $\lambda_\parallel$); (D) radial diffusivity (RD or $\lambda_\perp$); (E) reconstructed fiber numbers using DTI; and (F) diameters of optic nerves in the young and old groups of rhesus monkeys. Young, the young group; Old, the old group; mean, mean value; SD, standard deviation; y, year.

there was a systematic side bias in the measures. Measures for the two optic nerves were then averaged for each subject, and Student's t-tests for independent samples were carried out to assess the differences between the young and old adult monkeys to uncover aging-related changes of MD, FA, AD and RD.

Results

Paired t-tests of all 15 monkeys showed no significant differences in MD, AD, RD, FA, or optic-nerve diameter between the left and right optic nerves (P=0.81, 0.71, 0.81, 0.85, 0.19 and 0.64, respectively).

The age-related changes of the DTI-derived indices and the optic nerve diameters measured with T1-weighted images are shown in *Figure 2*. The most statistically reliable difference was in FA, which was 26.2% lower in the old monkeys than in the young adults (P=0.0087) (*Figure 2A*). The only other measure that approached significance was RD ($\lambda_\perp$) (*Figure 2D*), which was 44.3% higher in the
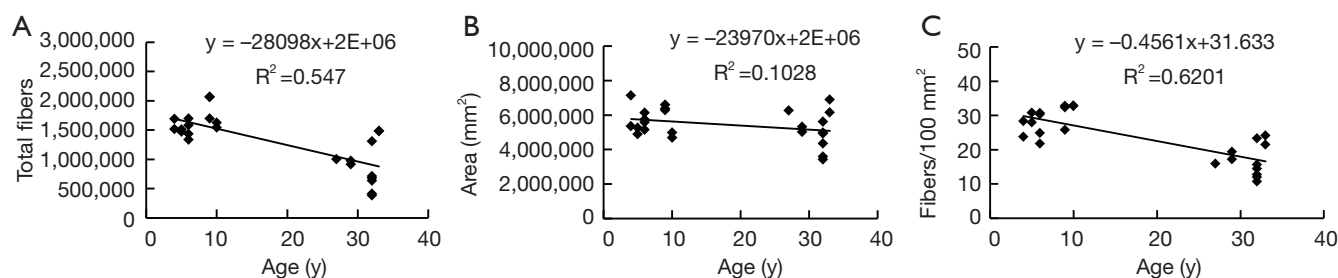
Figure 3 Data of Sandell and Peters (10) showing age-related changes in (A) total fiber number; (B) fiber area (cross-section area of optic nerve); and (C) fiber density of optic nerves in the young adult and old adult rhesus monkeys measured with light and electron microscopy. y, year.

old than in the young monkeys (P=0.058) (*Figure 2D*). Meanwhile, in comparison with the young group, MD and AD ($\lambda_{\parallel}$) of the old group were 24% (P=0.11) and 6.5% (P=0.47) higher (*Figure 2B,C*), and the mean fiber tract number and optic nerve diameter in the old group were –4.8% (P=0.24) and –3.5% (P=0.55) lower (*Figure 2E,F*), respectively. Obviously, there were no significant group differences in MD, AD ($\lambda_{\parallel}$), fiber tract number, or optic nerve diameter.

Discussion

Light and electron microscopic methods have previously been used to evaluate optic nerve aging in humans (1,8,49) and monkeys (9,10). *In vivo* optic nerve studies of age-related eye diseases in rodents and humans have been explored with DTI in recent years. To our knowledge, this is the first DTI study to characterize the normal aging effect of the optic nerve *in vivo* in large animals or NHPs.

White matter integrity can be compromised by fiber demyelination and axonal degeneration, which lead to FA decrease and/or diffusivity increase in animal and human brains (50-53). As seen in the present data, FA was significantly lower in the old monkey group, while RD ($\lambda_{\perp}$) was higher, although the latter difference statistically marginal (P=0.058). Experimental studies in rodent brains (37,54,55) have reported that degenerative changes in axons can result in decreased FA and decreased AD or $\lambda_{\parallel}$, the loss of axonal integrity and myelination yielding increased RD or $\lambda_{\perp}$. Thus, our DTI results could be interpreted as reflecting the age-related loss of optic nerve axons along with degenerative changes in myelin sheaths. Viewed in this way, our results are consistent with some of the main findings of Sandell and Peters (10), in their light- and electron-microscopic studies of postmortem rhesus tissue. As shown in *Figure 3*, the total fiber loss (–44.4%,

P<0.0001) and fiber density reduction (–41.1%, P <0.0001) from the previous microscopic study are in good agreement with the FA changes during aging in our DTI study. They reported that the average total number of optic nerve fibers was approximately 44% lower (0.9×10^6 versus 1.6×10^6) in a group of 27-30-year-old macaques compared to a group of 4-10-year-old macaques (10). In addition to fiber reduction, their study also reported degenerative changes in fiber sheaths that were most prevalent in the animals with the lowest fiber numbers. Similarly, aging in humans is associated with the loss of optic nerve fibers. For example, Dolman *et al*. revealed axon loss with increasing age that became particularly evident from 60 years upward (1). Jonas *et al*. investigated human optic nerve from 19 to 88 years old and found that the nerve fiber count decreased significantly with age with a linear annual loss of about 4,000 fibers staring at a calculated original population of about 1.4×10^6 fibers at birth (8).

Although our *in vivo* DTI results are largely congruent with results from postmortem histology, there are also disparities. For example, we observed no statistically significant difference in number of DTI-derived streamlines in the young versus old macaques, while the postmortem macaque and human studies report large differences in fiber numbers. This suggests that the numbers of DTI-derived streamlines may not be strongly correlated with the numbers of axons in a fiber tract as the DTI-based fiber tracking technique allows the visualization of fiber bundles and functional connectivity in brain central nervous system but cannot reconstruct the actual fibers (56). Furthermore, while we observed a robust difference in FA between the old and young group, the difference in RD or $\lambda_{\perp}$ was statistically marginal, and there was no difference in AD or $\lambda_{\parallel}$. Based on the work of Song and colleagues (37,54,55), we would expect that loss of axons and myelin integrity would result in reduced AD. It is possible that the failure to find a

difference in AD in the present study reflects small samples and inadequate statistical power or lack of subjects aged 27 years old or more in the old group. This could also account for the lack of an age-related difference in optic-nerve diameter in our MRI study (*Figure 2F*).

In addition, the scatterplots in *Figures 2* and *3* may illustrate the tendency of the parameters from MRI and light and electron microscopy examination during optic nerve aging. However, due to the lack of middle-aged animals in the present or previous study, the linear fits suggesting the alteration of these parameters between the young and old animals during optic nerve aging should be considered tentative. Also, it should be noted that involuntary eye movement in isoflurane-anesthetized animals may cause motion artifact in MRI images of eyes and retinas (57,58). In the present study, the eyeball was nearly invisible in the diffusion-weighted raw images as the water signal in the eyeball was suppressed due to the applied diffusion gradient (b =1,000 s/mm^2). In contrast, the eyeball movement was still visible in some raw b0 images (acquired with b =0 s/mm^2) of DTI scans. But no motion artifact was observed in the diffusion weighted images of the interested optic nerve section, indicating the involuntary eye movement didn't affect the DTI examinartion of the optic nerve in the present study.

Due to the limited spatial resolution of the DTI images, the DTI measures of optic nerve might be contaminated with the partial volume effect (PVE) from the surrounding cerebrospinal fluid (CSF) (59,60). In our present study, we used the proposed ROI selection procedure to mitigate the adverse effect. Also, as no significant reduction (–3.5%, P=0.55) was seen between the mean optic nerve diameters of the young and old adult monkeys (*Figure 2F*) in agreement with the fiber area change (–10%, P=0.16, *Figure 3B*), we believe that the DTI index changes observed in our study are age-related but not due to the PVE contributions from the diameter difference of optic nerve bundles between the young and old adult monkeys.

DTI is increasingly used in studying the optic nerve related diseases (24-27,35,37) and optic nerve development (36). With the advent of high field MRI and fast imaging technique, the DTI examination in diagnostic application of the optic nerve is becoming more widespread. Therefore, the present study of rhesus monkey optic nerves may provide a translationally relevant imaging protocol and also a normal reference baseline for studying the optic nerve related diseases in clinical settings.

In conclusion, this study demonstrates DTI can be a robust means to evaluate the optic nerve aging in a clinic setting. A substantial and significant decrease of FA (P<0.01) in the optic nerve was observed, highly consistent with the previous findings of fiber loss in a light and electron microscopic study, suggesting FA is sensitive to aging effect and may be used for quantitatively characterizing the optic nerve abnormality in aging or age-related vision diseases.

Acknowledgements

References

1. Dolman CL, McCormick AQ, Drance SM. Aging of the optic nerve. Arch Ophthalmol 1980;98:2053-8.
2. Quigley HA, Dunkelberger GR, Green WR. Retinal ganglion cell atrophy correlated with automated perimetry in human eyes with glaucoma. Am J Ophthalmol 1989;107:453-64.
3. Harwerth RS, Wheat JL, Rangaswamy NV. Age-related losses of retinal ganglion cells and axons. Invest Ophthalmol Vis Sci 2008;49:4437-43.
4. Weinreb RN, Khaw PT. Primary open-angle glaucoma. Lancet 2004;363:1711-20.
5. Tezel G, Luo C, Yang X. Accelerated aging in glaucoma: immunohistochemical assessment of advanced glycation end products in the human retina and optic nerve head. Invest Ophthalmol Vis Sci 2007;48:1201-11.
6. See JL, Nicolela MT, Chauhan BC. Rates of neuroretinal rim and peripapillary atrophy area change: a comparative study of glaucoma patients and normal controls. Ophthalmology 2009;116:840-7.
7. Gupta N, Yucel YH. Glaucoma as a neurodegenerative disease. Curr Opin Ophthalmol 2007;18:110-4.
8. Jonas JB, Schmidt AM, Muller-Bergh JA, et al. Human optic nerve fiber count and optic disc size. Invest Ophthalmol Vis Sci 1992;33:2012-8.
9. Morrison JC, Cork LC, Dunkelberger GR, et al. Aging

changes of the rhesus monkey optic nerve. Invest Ophthalmol Vis Sci 1990;31:1623-7.

10. Sandell JH, Peters A. Effects of age on nerve fibers in the rhesus monkey optic nerve. J Comp Neurol 2001;429:541-53.

11. Peters A. The effects of normal aging on myelinated nerve fibers in monkey central nervous system. Front Neuroanat 2009;3:11.

12. Cepurna WO, Kayton RJ, Johnson EC, et al. Age related optic nerve axonal loss in adult Brown Norway rats. Exp Eye Res 2005;80:877-84.

13. Le Bihan D, Mangin JF, Poupon C, et al. Diffusion tensor imaging: concepts and applications. J Magn Reson Imaging 2001;13:534-46.

14. Alexander AL, Lee JE, Lazar M, et al. Diffusion tensor imaging of the brain. Neurotherapeutics 2007;4:316-29.

15. Hermoye L, Saint-Martin C, Cosnard G, et al. Pediatric diffusion tensor imaging: normal database and observation of the white matter maturation in early childhood. Neuroimage 2006;29:493-504.

16. Hüppi PS, Dubois J. Diffusion tensor imaging of brain development. Semin Fetal Neonatal Med 2006;11:489-97.

17. Thomason ME, Thompson PM. Diffusion imaging, white matter, and psychopathology. Annu Rev Clin Psychol 2011;7:63-85.

18. Pavuluri MN, Yang S, Kamineni K, et al. Diffusion tensor imaging study of white matter fiber tracts in pediatric bipolar disorder and attention-deficit/hyperactivity disorder. Biol Psychiatry 2009;65:586-93.

19. Lebel C, Gee M, Camicioli R, et al. Diffusion tensor imaging of white matter tract evolution over the lifespan. Neuroimage 2012;60:340-52.

20. Luk G, Bialystok E, Craik FI, et al. Lifelong bilingualism maintains white matter integrity in older adults. J Neurosci 2011;31:16808-13.

21. Meier IB, Manly JJ, Provenzano FA, et al. White matter predictors of cognitive functioning in older adults. J Int Neuropsychol Soc 2012;18:414-27.

22. Rogalski E, Stebbins GT, Barnes CA, et al. Age-related changes in parahippocampal white matter integrity: a diffusion tensor imaging study. Neuropsychologia 2012;50:1759-65.

23. Holt JL, Kraft-Terry SD, Chang L. Neuroimaging studies of the aging HIV-1-infected brain. J Neurovirol 2012;18:291-302.

24. Trip SA, Wheeler-Kingshott C, Jones SJ, et al. Optic nerve diffusion tensor imaging in optic neuritis. Neuroimage 2006;30:498-505.

25. Xu J, Sun SW, Naismith RT, et al. Assessing optic nerve pathology with diffusion MRI: from mouse to human. NMR Biomed 2008;21:928-40.

26. Kolbe S, Chapman C, Nguyen T, et al. Optic nerve diffusion changes and atrophy jointly predict visual dysfunction after optic neuritis. Neuroimage 2009;45:679-86.

27. Salmela MB, Cauley KA, Nickerson JP, et al. Magnetic resonance diffusion tensor imaging (MRDTI) and tractography in children with septo-optic dysplasia. Pediatr Radiol 2010;40:708-13.

28. Salmela MB, Cauley KA, Andrews T, et al. Magnetic resonance diffusion tensor imaging of the optic nerves to guide treatment of pediatric suprasellar tumors. Pediatr Neurosurg 2009;45:467-71.

29. Li J, Shi W, Li M, et al. Time-dependent diffusion tensor changes of optic nerve in patients with indirect traumatic optic neuropathy. Acta Radiol 2013. [Epub ahead of print].

30. Chang ST, Xu J, Trinkaus K, et al. Optic Nerve Diffusion Tensor Imaging Parameters and Their Correlation With Optic Disc Topography and Disease Severity in Adult Glaucoma Patients and Controls. J Glaucoma 2013. [Epub ahead of print].

31. Wang MY, Wu K, Xu JM, et al. Quantitative 3-T diffusion tensor imaging in detecting optic nerve degeneration in patients with glaucoma: association with retinal nerve fiber layer thickness and clinical severity. Neuroradiology 2013;55:493-8.

32. Engelhorn T, Michelson G, Waerntges S, et al. Changes of radial diffusivity and fractional anisotropy in the optic nerve and optic radiation of glaucoma patients. ScientificWorldJournal 2012;2012:849632.

33. Nucci C, Mancino R, Martucci A, et al. 3-T Diffusion tensor imaging of the optic nerve in subjects with glaucoma: correlation with GDx-VCC, HRT-III and Stratus optical coherence tomography findings. Br J Ophthalmol 2012;96:976-80.

34. Wheeler-Kingshott CA, Trip SA, Symms MR, et al. In vivo diffusion tensor imaging of the human optic nerve: pilot study in normal controls. Magn Reson Med 2006;56:446-451.

35. Coimbra A, Ogidigben M, Peiffer R, et al. Using MRI to quantify optic nerve injury in monkeys with experimental glaucoma: atrophy and fiffusivity effects. In: Proceedings of the 17th Annual Meeting of ISMRM, Honolulu, Hawaii, 2009:Abstract 1074.

36. Yan Y, Nair G, Li L, et al. In vivo evaluation of optic nerve development in non-human primates by using diffusion

tensor imaging. Int J Dev Neurosci 2014;32;64-8.

37. Song SK, Sun SW, Ju WK, et al. Diffusion tensor imaging detects and differentiates axon and myelin degeneration in mouse optic nerve after retinal ischemia. Neuroimage 2003;20:1714-22.

38. Thuen M, Olsen O, Berry M, et al. Combination of Mn(2+)-enhanced and diffusion tensor MR imaging gives complementary information about injury and regeneration in the adult rat optic nerve. J Magn Reson Imaging 2009;29:39-51.

39. Hui ES, Fu QL, So KF, et al. Diffusion tensor MR study of optic nerve degeneration in glaucoma. Conf Proc IEEE Eng Med Biol Soc 2007;2007:4312-5.

40. Wang Q, Vlkolinsky R, Xie M, et al. Diffusion tensor imaging detected optic nerve injury correlates with decreased compound action potentials after murine retinal ischemia. Invest Ophthalmol Vis Sci 2012;53:136-42.

41. Chan KC, Cheng JS, Fan S, et al. In vivo evaluation of retinal and callosal projections in early postnatal development and plasticity using manganese-enhanced MRI and diffusion tensor imaging. Neuroimage 2012;59:2274-83.

42. Levkovitch-Verbin H. Animal models of optic nerve diseases. Eye (Lond) 2004;18:1066-74.

43. Preuss TM. Specializations of the human visual system: the monkey model meets human reality. In: Kaas JH, Collins CE. eds. The Primate Visual System. Boca Raton, FL: CRC Press, 2004:231-59.

44. Sandell JH, Peters A. Effects of age on the glial cells in the rhesus monkey optic nerve. J Comp Neurol 2002;445:13-28.

45. Yang H, Downs JC, Burgoyne CF. Physiologic intereye differences in monkey optic nerve head architecture and their relation to changes in early experimental glaucoma. Invest Ophthalmol Vis Sci 2009;50:224-34.

46. Marner L, Nyengaard JR, Tang Y, et al. Marked loss of myelinated nerve fibers in the human brain with age. J Comp Neurol 2003;462:144-52.

47. Li CX, Patel S, Auerbach EJ, et al. Dose-dependent effect of isoflurane on regional cerebral blood flow in anesthetized macaque monkeys. Neurosci Lett 2013;541:58-62.

48. Andersson JL, Skare S, Ashburner J. How to correct susceptibility distortions in spin-echo echo-planar images: application to diffusion tensor imaging. Neuroimage 2003;20:870-88.

49. Sylvester PE, Ari K. The size and growth of the human optic nerve. J Neurol Neurosurg Psychiatry 1961;24:45-9.

50. Sotak CH. The role of diffusion tensor imaging in the evaluation of ischemic brain injury - a review. NMR Biomed 2002;15:561-9.

51. Le Bihan D, Johansen-Berg H. Diffusion MRI at 25: exploring brain tissue structure and function. Neuroimage 2012;61:324-41.

52. Salat DH, Tuch DS, Greve DN, et al. Age-related alterations in white matter microstructure measured by diffusion tensor imaging. Neurobiol Aging 2005;26:1215-27.

53. Bennett IJ, Madden DJ, Vaidya CJ, et al. Age-related differences in multiple measures of white matter integrity: A diffusion tensor imaging study of healthy aging. Hum Brain Mapp 2010;31:378-90.

54. Song SK, Sun SW, Ramsbottom MJ, et al. Dysmyelination revealed through MRI as increased radial (but unchanged axial) diffusion of water. Neuroimage 2002;17:1429-36.

55. Song SK, Yoshino J, Le TQ, et al. Demyelination increases radial diffusivity in corpus callosum of mouse brain. Neuroimage 2005;26:132-40.

56. Mori S, van Zijl PC. Fiber tracking: principles and strategies - a technical review. NMR Biomed 2002;15:468-80.

57. Nair G, Kim M, Nagaoka T, et al. Effects of common anesthetics on eye movement and electroretinogram. Doc Ophthalmol 2011;122:163-76.

58. Zhang X, Li Y, Duong TQ. Image Instability Evaluation and Motion Correction for High-resolution MRI of the Rat Retina. In: Proceedings of the 17th Annual Meeting of ISMRM, Honolulu, Hawaii, 2009:Abstract 4600.

59. Ma X, Kadah YM, LaConte SM, et al. Enhancing measured diffusion anisotropy in gray matter by eliminating CSF contamination with FLAIR. Magn Reson Med 2004;51:423-7.

60. Vos SB, Jones DK, Viergever MA, et al. Partial volume effect as a hidden covariate in DTI analyses. Neuroimage 2011;55:1566-76.